A&A 403, 593–604 (2003)
DOI: 10.1051/0004-6361:20021739

Astronomy & Astrophysics

Spiral and shock front development in accretion discs in close binaries: Physically viscous and non-viscous SPH modelling

G. Lanzafame⋆

INAF - Osservatorio Astrofisico di Catania, Via S. Sofia 78, 95123 Catania, Italy

Received 2 April 2002 / Accepted 5 November 2002

Abstract. A comparison between an accretion disc model, whose transport mechanisms are driven only by artificial viscosity, and a physically viscous accretion disc model for the same close binary system is performed here by adopting the same parameters and boundary conditions. These assumptions mean that artificial viscosity, included in both models, shares, together with physical viscosity, mass and angular momentum transport in the second disc model. The Smooth Particle Hydrodynamics (SPH) Lagrangian scheme has been adopted in both models and $\alpha_{ss} = 1$ has been considered as for the viscous model according to the well-known Shakura and Sunjaev formulation. Physical viscosity is represented by the viscous force contribution as a divergence of the symmetric viscous stress tensor in the Navier-Stokes equation, whilst the viscous energy contribution is given by a symmetric combination of the symmetric shear tensor times to the particle velocity. Adopting a supersonic particle inflowing at the inner lagrangian point L1, clear spiral strong shocks in the radial flux develop from the inviscid 3D model. Extended spirals and shock fronts are even more evident in the viscous accretion disc model, which is larger than the non-viscous one in the *XY* orbital plane. Characteristics of the two disc structures as well as observational consequences are discussed.

Key words. accretion, accretion disks – stars: binaries: close – methods: numerical – shock waves

1. Introduction

The problem of the development of spirals in the radial flow of spiral shocks in physically inviscid accretion discs has been studied by various authors: Sawada et al. (1987), Spruit et al. (1987), Kaisig (1989), Matsuda et al. (1990, 1992), Ichikawa & Osaki (1992, 1994), Sawada & Matsuda (1992), Savonije et al. (1994), Lanzafame & Belvedere (1997, 1998), Murray (1996), Yukawa et al. (1997), Bisikalo et al. (1998a,b, 1999), Blondin (2000), Lanzafame et al. (2000, 2001), Makita et al. (2000), Lanzafame & Belvedere (2001), Truss et al. (2001), Belvedere & Lanzafame (2002). Common opinion supported in many of such papers is that outer edge perturbations are responsible for spiral pattern structure generation. However, our conclusions, as for the origin of such perturbations, differ from those of other authors. In fact, Lanzafame et al. (2000) and in particular Lanzafame et al. (2001), showed that high angular momentum and kinematic energy inflowing conditions at the L1 point are responsible for spirals and shock formation through collisional perturbations at the disc outer edge. Such perturbations, at least in 2D modelling, are generated by the injected flow in the L1 point. The same conclusion was also claimed by Bisikalo et al. (1998a,b, 1999) even if these authors conclude that the injection velocity only can influence the disc flow structure. Of course we cannot exclude that tidal perturbations at the disc outer edge can support such spiral patterns, but we support the idea that tidal torque is not the main cause. Among the mentioned authors, Ickikawa & Osaki (1994) themselves admit that the inclusion of pressure and viscosity effects are important to have a better understanding of such structures.

To address this issue, in this work we compare structure, dynamics and energetics of a 3D Smooth Particle Hydrodynamics (SPH) physically inviscid accretion disc model with a 3D SPH physically viscous one of the same close binary system. These two models are built by adopting the same simple boundary conditions at the disc inner and outer edges and the same high gas compressibility. At the same time we consider highly supersonic injection conditions at the inner lagrangian point L1 to verify, once more, that high angular momentum injection conditions support evident spiral structures and spiral shocks in the radial velocity flux, as it was evidenced in physically inviscid SPH 2D models by Lanzafame et al. (2000, 2001). These assumptions mean that artificial viscosity, included in both models as a common boundary condition, shares, together with physical viscosity, mass and angular momentum transport in the second disc model. In 2D models the shadowing effect due to artificial viscosity is lighter than in 3D models where weak spiral shocks can be masked in the disc bulk (Monaghan 1985, 1992; Monaghan & Lattanzio 1985), For this reason the investigations are generally limited to the strong shock case. Limitations of the models depend also on gas compressibility: low compressibility models suffer of a low resolution due to the low particle concentration, whilst in high

⋆ e-mail: glanzafame@astrct.ct.astro.it

compressibility models the smoothing effect due to artificial viscosity is stressed because of the high particle concentration.

Before starting this work, we knew that spirals and shock fronts would have developed in 2D SPH models (Lanzafame et al. 2000, 2001), but we did not know if they would have still developed in 3D SPH inviscid models and, especially, in models including high physical viscosity. In fact, other authors such as Flebbe et al. (1992, 1994), Bisikalo et al. (2000), who also included physical viscosity, did not mention anything about the existence of spirals and spiral shocks in their models.

The SPH formulation of viscous contributions both in the Navier-Stokes and in the energy equations has been developed by Flebbe et al. (1992, 1994). Such a SPH formulation of general viscous forces could also describe both molecular and turbulent viscosity effects (Landau & Lifschitz 1959). These goals are not obtained by the artificial viscosity which is, however, introduced in both models to resolve shocks numerically and to avoid spurious heating, artificial viscosity that vanishes when the particle interpolation domain reduces, in the limit, zero. Drimmell (1993), Meglicki et al. (1993) and Murray (1996) demonstrated that the linear component of the artificial viscosity by itself, in the continuum limit, yields a viscous shear force. In particular the last two authors have written explicitly such artificial viscosity contribution both in the momentum equation and in the energy equation. Moreover, Murray (1996) found a nice analogy between the shear viscosity generated by the linear artificial viscosity term and the well-known Shakura and Sunyaev shear viscosity, in the continuum limit. These conclusions do not disagree with our goals. In fact we realize that the SPH method, like other finite difference schemes, is far from the continuum limit; moreover we need the quadratic (β) artificial viscosity term to handle strong shocks. In conclusion, we compare two SPH accretion disc models where artificial viscosity is necessary in both discs as a common boundary condition. One disc model includes physical viscosity, whilst the other one does not. In this paper, the viscous force contribution is represented as a divergence of the symmetric viscous stress tensor in the Navier-Stokes equation. A symmetric combination of the symmetric shear tensor times to the particle velocity has been added to the energy equation as a viscous heating contribution. The bulk physical viscosity contribution has not been considered for the sake of simplicity.

In Sect. 2 of this paper we briefly present the SPH formulation of both models. In Sect. 3 we describe the boundary conditions adopted in the accretion disc models in the close binary system considered and the physical characteristics of disc gas adopted, whilst in Sect. 4 we discuss our results and some possible observational consequences which can be attributed to the two models.

2. SPH formulation of viscous perfect gas hydrodynamics

As for non-viscous gas hydrodynamics, the relevant equations to our model are:

$$\frac{\mathrm{d}\rho}{\mathrm{d}t} + \rho\nabla\cdot\underline{v} = 0 \qquad \text{continuity equation (1)}$$

$$\frac{\mathrm{d}\underline{v}}{\mathrm{d}t} = -\frac{\nabla p}{\rho} + [-2\underline{\omega}\times\underline{v} + \underline{\omega}\times(\underline{\omega}\times\underline{r}) - \nabla\Phi_{\mathrm{grav}}]$$

momentum equation (2)

$$\frac{\mathrm{d}\epsilon}{\mathrm{d}t} = -\frac{p}{\rho}\nabla\cdot\underline{v} \qquad \text{energy equation (3)}$$

$$p = (\gamma-1)\rho\epsilon. \qquad \text{perfect gas equation (4)}$$

Here most symbols have the usual meaning, d/dt stands for the Lagrangian derivative, ρ is the gas density, ϵ is the thermal energy per unit mass, Φ_{grav} is the effective gravitational potential due to the two stars and $\underline{\omega}$ is the angular velocity of the rotating reference frame, corresponding to the rotational period of the binary system. Self gravitation has not been included, as it appears irrelevant. The adiabatic index γ has the meaning of a numerical parameter whose value lies in the limit between 1 and 5/3, in principle.

The SPH method is a lagrangian scheme that discretizes the fluid into moving interacting and interpolating domains called "particles". All particles move according to pressure and body forces. The method makes use of a Kernel W useful to interpolate a physical quantity $A(\underline{r})$ related to a gas particle at position $\underline{r}$ according to:

$$A(\underline{r}) = \int_D A(\underline{r}')W(\underline{r},\underline{r}',h)\mathrm{d}\underline{r}' \tag{5}$$

$W(\underline{r},\underline{r}',h)$, the interpolation Kernel, is a continuous function – or two connecting continuous functions whose derivatives are continuous even at the connecting point – defined in the spatial range $2h$, whose limit for $h\to 0$ is the delta Dirac distribution function. All physical quantities are described as extensive properties smoothly distributed in space and computed by interpolation at $\underline{r}$. In SPH terms we write:

$$A_i = \sum_{j=1}^{N}\frac{A_j}{n_j}W(\underline{r}_i,\underline{r}_j,h) \tag{6}$$

where the sum is extended to all particles included in the domain D, $n_j = \rho_j/m_j$ is the number density relative to the jth particle and $W(\underline{r}_i,\underline{r}_j,h)\le 1$ is the adopted interpolation Kernel whose value is determined by the relative distance between particles i and j.

In SPH formalism, Eqs. (2) and (3) take the form:

$$\frac{\mathrm{d}\underline{v}_i}{\mathrm{d}t} = -\sum_{j=1}^{N} m_j\left(\frac{p_i}{\rho_i^2}+\frac{p_j}{\rho_j^2}\right)\nabla_i W_{ij} + \underline{g}_i \tag{7}$$

$$\frac{\mathrm{d}\epsilon_i}{\mathrm{d}t} = \frac{1}{2}\sum_{j=1}^{N} m_j\left(\frac{p_i}{\rho_i^2}+\frac{p_j}{\rho_j^2}\right)\underline{v}_{ij}\cdot\nabla_i W_{ij} \tag{8}$$

where $\underline{g}_i = -2\underline{\omega}\times\underline{v}_i + \underline{\omega}\times(\underline{\omega}\times\underline{r}_i) - \nabla\Phi_{\mathrm{grav},i}$, $\underline{v}_{ij} = \underline{v}_i - \underline{v}_j$ and m_j is the mass of jth particle. Alternatively, Eq. (8) can also be written:

$$\frac{\mathrm{d}\epsilon_i}{\mathrm{d}t} = \sum_{j=1}^{N} m_j\frac{p_i}{\rho_i^2}\underline{v}_{ij}\cdot\nabla_i W_{ij}. \tag{9}$$

In this scheme the continuity equation takes the form:

$$\frac{\mathrm{d}\rho_i}{\mathrm{d}t} = -\sum_{j=1}^{N} m_j \underline{v}_{ij} \cdot \nabla_i W_{ij} \tag{10}$$

or, as we prefer, it can be written as:

$$\rho_i = \sum_{j=1}^{N} m_j W_{ij} \tag{11}$$

which identifies the natural space interpolation of particle densities according to Eq. (6).

The pressure term includes the artificial viscosity contribution given by Monaghan (1985, 1992) and Monaghan & Lattanzio (1985), with an appropriate thermal diffusion term which reduces shock fluctuations. It is given by:

$$\eta_{ij} = \alpha\mu_{ij} + \beta\mu_{ij}^2 \tag{12}$$

where

$$\mu_{ij} = \frac{2h\underline{v}_{ij} \cdot \underline{r}_{ij}}{(c_{si} + c_{sj})(r_{ij}^2 + \xi)} \tag{13}$$

with c_{si} being the sound speed of the ith particle, $\underline{r}_{ij} = \underline{r}_i - \underline{r}_j$, $\xi^2 \ll h^2$, $\alpha \approx 1$ and $\beta \approx 2$. α and β parameters of the order of unity are usually adopted to dampen oscillations behind high Mach number shock fronts developed by non-linear instabilities (Boris & Book 1973). These α and β values were also adopted by Lattanzio et al. (1986). Lower α and β values, as adopted by Meglicki et al. (1993), would develop more turbulence in the disc and possibly only one shock front at the impact zone between the infalling particle stream and the returning particle stream at the disc outer edge. In the physically inviscid SPH gas dynamics, angular momentum transport is mainly due to the artificial viscosity included in the pressure terms as:

$$\frac{p_i}{\rho_i^2} + \frac{p_j}{\rho_j^2} = \left(\frac{p_i^{(G)}}{\rho_i^2} + \frac{p_j^{(G)}}{\rho_j^2}\right)(1 + \eta_{ij}) \tag{14}$$

where $p^{(G)}$ is the intrinsic gas pressure.

As far as Lagrangian SPH modelling of viscous gas dynamics is concerned, we have to add the viscous force to the right side of momentum Eq. (2). The resulting Navier-Stokes equation is:

$$\frac{\mathrm{d}\underline{v}}{\mathrm{d}t} = -\frac{\nabla p}{\rho} + [-2\underline{\omega} \times \underline{v} + \underline{\omega} \times (\underline{\omega} \times \underline{r}) - \nabla\Phi_{\mathrm{grav}}] + \frac{1}{\rho}\nabla \cdot t. \tag{15}$$

Here, the viscous stress tensor $t_{\alpha\beta}$ includes the positive first and second viscosity coefficients η_{v} and ζ_{v} which are velocity independent and describing shear and tangential viscosity stresses (η_{v}) and compressibility stresses (ζ_{v}):

$$t_{\alpha\beta} = \eta_{\mathrm{v}}\sigma_{\alpha\beta} + \zeta_{\mathrm{v}}\nabla \cdot \underline{v} \tag{16}$$

where the shear

$$\sigma_{\alpha\beta} = \frac{\partial v_\alpha}{\partial x_\beta} + \frac{\partial v_\beta}{\partial x_\alpha} - \frac{2}{3}\delta_{\alpha\beta}\nabla \cdot \underline{v}. \tag{17}$$

In these equations the indexes α and β are spatial indexes whilst tensors are written in bold characters. For the sake of simplicity we assume $\zeta_{\mathrm{v}} = 0$, however our code allows also different possibilities. As in Flebbe et al. (1992, 1994), defining

$$V_{i\alpha\beta} = \sum_{j=1}^{N} \frac{m_j \underline{v}_{ji\alpha}}{\rho_j} \frac{\partial W_{ij}}{\partial x_\beta} \tag{18}$$

as the SPH formulation of $\partial v_\alpha/\partial x_\beta$, the SPH equivalent of the shear is:

$$\sigma_{i\alpha\beta} = V_{i\alpha\beta} + V_{i\beta\alpha} - \frac{2}{3}\delta_{\alpha\beta}V_{i\gamma\gamma} \tag{19}$$

therefore, the SPH momentum equation equivalent is:

$$\begin{aligned}\frac{\mathrm{d}\underline{v}_i}{\mathrm{d}t} &= -\sum_{j=1}^{N} m_j \left(\frac{p_i}{\rho_i^2} + \frac{p_j}{\rho_j^2}\right)\nabla_i W_{ij} + \underline{g}_i \\ &+ \sum_{j=1}^{N} m_j \left(\frac{\eta_{vi}\boldsymbol{\sigma}_i}{\rho_i^2} + \frac{\eta_{vj}\boldsymbol{\sigma}_j}{\rho_j^2}\right) \cdot \nabla_i W_{ij}\end{aligned} \tag{20}$$

and the energy balance equation for the total energy $E = \epsilon + \frac{1}{2}v^2$ is:

$$\frac{\mathrm{d}}{\mathrm{d}t}\left(\epsilon + \frac{1}{2}v^2\right) = -\frac{1}{\rho}\left(p\nabla \cdot \underline{v} - \nabla \cdot \left(\underline{v} \cdot \mathbf{t}\right)\right) \tag{21}$$

which has the SPH equivalent:

$$\begin{aligned}\frac{\mathrm{d}}{\mathrm{d}t}E_i &= -\sum_{j=1}^{N} m_j \left(\frac{p_i\underline{v}_i}{\rho_i^2} + \frac{p_j\underline{v}_j}{\rho_j^2}\right) \cdot \nabla_i W_{ij} \\ &+ \sum_{j=1}^{N} m_j \left(\eta_{vi}\frac{\boldsymbol{\sigma}_i \cdot \underline{v}_i}{\rho_i^2} + \eta_{vj}\frac{\boldsymbol{\sigma}_j \cdot \underline{v}_j}{\rho_j^2}\right) \cdot \nabla_i W_{ij}\end{aligned} \tag{22}$$

where $E_i = (\epsilon_i + \frac{1}{2}v_i^2)$.

A full justification of this SPH formalism can be found in Flebbe et al. (1992, 1994).

3. Parameters and boundary conditions

The characteristics of the binary system are determined by the masses of the two companion stars and by their mutual distance. We chose to model a system in which both mass M_1 of the primary compact star and the mass M_2 of the secondary normal star are equal to one $M_\odot$ and the distance between their centres is $d_{12} = 10^6$ km. The injection gas velocity from the L1 point is fixed to $v_{\mathrm{inj}} \simeq 130\ \mathrm{km\,s^{-1}}$ whilst the injection gas temperature in L1 is fixed to $T_\circ = 10^4$ K. Such a temperature value is a bit higher than the value corresponding to a normal 1 $M_\odot$ star because, even as a first approximation, the radiative heating of the secondary surface due to lightening of the disc is taken into account. Gas compressibility is fixed by the adiabatic index γ of 1.01, an often used value (see e.g. Molteni et al. 1991; Lanzafame et al. 1992, 1993, 2000, 2001; Lanzafame & Belvedere 1997, 1998; Yukawa et al. 1997; Makita et al. 2000). We have chosen a highly supersonic injection velocity at the L1 point at the upper velocity limit normally considered, to verify if, adopting a high angular momentum injection condition, spiral structures and shocks in the radial flow appears in

3D disc modelling as shown in Lanzafame et al. (2000, 2001) in 2D disc modelling. In fact, we and other authors (Meglicki et al. 1993; Yukawa et al. 1997) have found that spirals and shock fronts in the radial flux do not develop in high compressibility 3D SPH accretion disc models adopting sonic injection conditions in L1, in spite of the fact that tidally induced spiral patterns should be developed (Blondin 2000; Murray 1996; Truss et al. 2001), at least in 2D modelling. Therefore, our assumption of strongly supersonic mass inflow should be effective enough to allow spirals to form in spite of artificial viscosity degradation. In our models we have as unknowns: pressure, density, temperature, velocity, so we solve the continuity, momentum, energy, and state (perfect gas) equations. $\gamma = 1.01$ simulates a physical situation of local equilibium between energy inputs and outputs. This does not mean that the discs are isothermal. Indeed, a temperature gradient exists in the discs and the results worked out in Lanzafame et al. (1992), Yukawa et al. (1997), as for inviscid disc models, show that it is in good agreement in the disc bulk with the standard analytical models. We agree that our models could be improved including radiative losses and transport. However, low γ models are realistic enough in our opinion because they are able to point out the differences in disc structure and dynamics induced by the kinematical constraints. Moreover, the large particle number for $\gamma = 1.01$ determines a better resolution and statistics than the higher γs, even if the degradation effect of artificial viscosity on shock fronts is stronger in the disc bulk.

In order to make our equations dimensionless, we adopted the following normalization factors: $M = M_1 + M_2$ for masses, $d_2 = 10^{11}$ cm for lengths, $v_\circ = \sqrt{G\,(M_1 + M_2)/d_{12}}$ for speeds, so that the orbital period is normalized to 2π, $\rho_\circ = 10^{-9}$ g cm^{-3} for the density, $p_\circ = \rho_\circ v_\circ^2$ dyn cm^{-2} for pressure, $v_\circ^2$ for thermal energy per unit mass and $T_\circ = (\gamma - 1)v_\circ^2\, m_\mathrm{p}\, K_\mathrm{B}^{-1}$ for temperature, where m_p is the proton mass and K_B is the Boltzman constant. The adopted Kernel width in the SPH interpolations is $h = 0.005$ and the geometrical domain including moving disc particles is a sphere of radius 0.6, centred on the primary. The rotating reference frame is centred on the compact primary and its rotational period equals the orbital one. We simulated the physical conditions at the inner and at the outer edges as follows:

a) inner edge:
the free inflow condition is realized by eliminating particles flowing inside the sphere of radius 4*h*, centred on the primary. It follows that disc structure and dynamics are altered a few *h* values near the inner edge, adopting a fixed *h* SPH code, but these alterations in disc behaviour are relatively small because they are counterbalanced by a good particle concentration close to the inner edge in the supersonic injection models.

b) outer edge:
the injection of "new" particles from L1 towards the interior of the primary Roche Lobe is simulated by generating them in fixed points, called "injectors", symmetrically placed within an angle having the L1 point as a vertex and an aperture of $\sim 57^\circ$. The initial injection particle velocity is radial with respect to the L1 point. In order to simulate a constant and smooth gas injection, a "new" particle is generated in the injectors whenever "old" particles leave an injector free, inside a small sphere with radius *h*, centred on the injector itself.

The formulation adopted as for the 3D SPH accretion disc model including physical viscosity is the well-known Shakura (1972) and Shakura & Sunyaev (1973) α_{ss} parametrization: $\nu = \alpha_{\mathrm{ss}} c_\mathrm{s} H$, where c_s is the sound velocity, $0 \leq \alpha_{\mathrm{ss}} \leq 1$ is the Shakura and Sunyaev parameter and $H = r_{xy} c_\mathrm{s} / \sqrt{M_1 / r_{xy}}$ is a dimensionless estimate of the standard disc thickness, where $r_{xy} = \sqrt{X_i^2 + Y_i^2}$ is the cylindrical radial coordinate of the *i*th particle. In this paper we chose to adopt $\alpha_{\mathrm{ss}} = 1$ to point out evident differences in disc structure and dynamics between the two SPH disc models. Of course, in principle, each positive value of $\alpha_{\mathrm{ss}} \leq 1$ value could be adopted. Nevertheless, physically viscous models whose $\alpha_{\mathrm{ss}} \leq 0.2$ show weak differences in disc structures, dynamics, energetics and in accretion rates in comparison to physically inviscid disc models. In fact a previous simulation, performed by us adopting $\alpha_{\mathrm{ss}} = 0.1$, did not produce such evident differences.

4. Results and discussion

We carried out our simulations until time $t = 22 \simeq 3.5$ orbital periods trying to get a fully stationary configuration where particle injection from the L1 point statistically balances particle accretion from the inner edge and particle ejection from the outer edge. In reality, we chose to interrupt our calculations at that time because we realized that, due to the very high injection rate and to the high gas compressibility ($\gamma = 1.01$), this condition can be asymptotically achieved for both models. Nothwithstanding, disc structures are well defined at $t = 22$ and are stable enough after 8 months of cpu time working with a Compaq Alpha XP1000.

4.1. 3D SPH spirals in inviscid model

Figure 1 shows *XY* and *XZ* plots of physically inviscid (left side) and physically viscous (right side) accretion disc structures. While the *XY* plot of the physically viscous model shows clearly the development of the spiral structures, the equivalent plot for the physically inviscid model of the accretion disc does not show clearly enough such effect. The appearence of the structure, that is masked in the left hand side of Fig. 1, shows up clearly in Fig. 2, where only the supersonic components of the radial velocity flux are presented in the *XY* plots. The same evidence is also clearly shown in Fig. 3. In such a figure, on the same scale of Figs. 1 and 2, the spiralling kinematical structure of the subsonic components (only for the physically inviscid model) is clearly visible. In the four subplots selections of SPH disc particles are shown having radial Mach number between $0 \div 0.25$, $0.25 \div 0.50$, $0.50 \div 0.75$, $0.75 \div 1$. Beside the existence of the spiral structures, Fig. 3 shows also that disc particles, subsonic in the radial flux, whose radial Mach number M_r approaches 1 are mainly confined at the disc outer edge.

A first relevant result to notice is that for the first time a 3D SPH physically inviscid accretion disc model has been obtained showing spiral shocks in the radial flux at the outer edge in the L1 inflowing case. In previous papers,

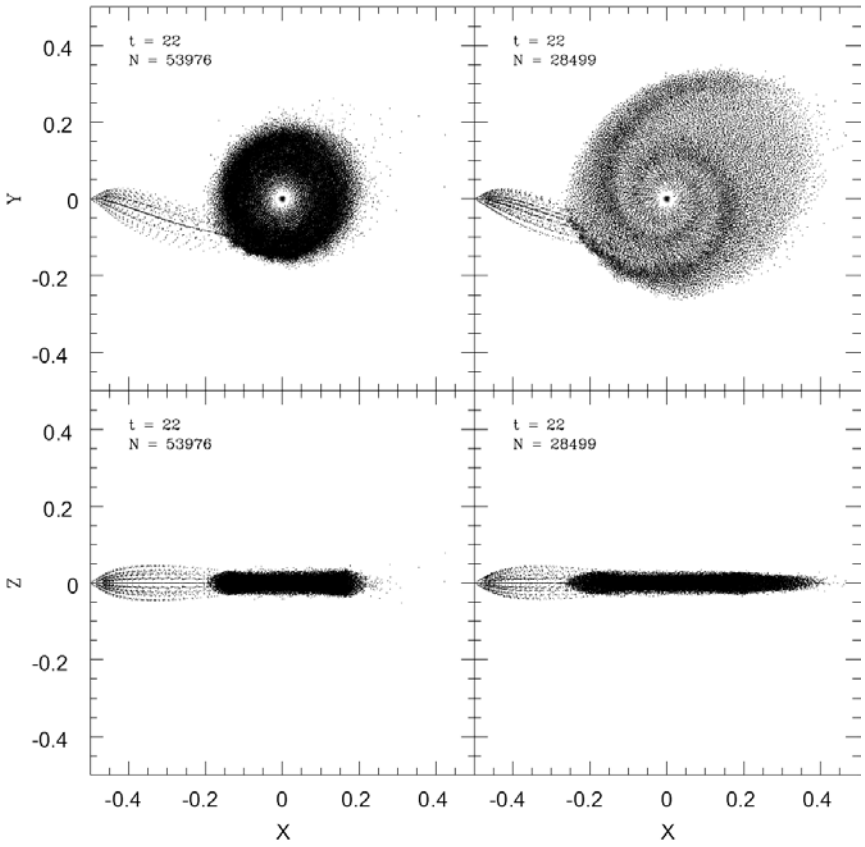

Fig. 1. *XY* and *XZ* plots of the "inviscid" SPH accretion disc model (left side) and the physically viscous one (right side). Final time *t* and total particle number *N* are reported.

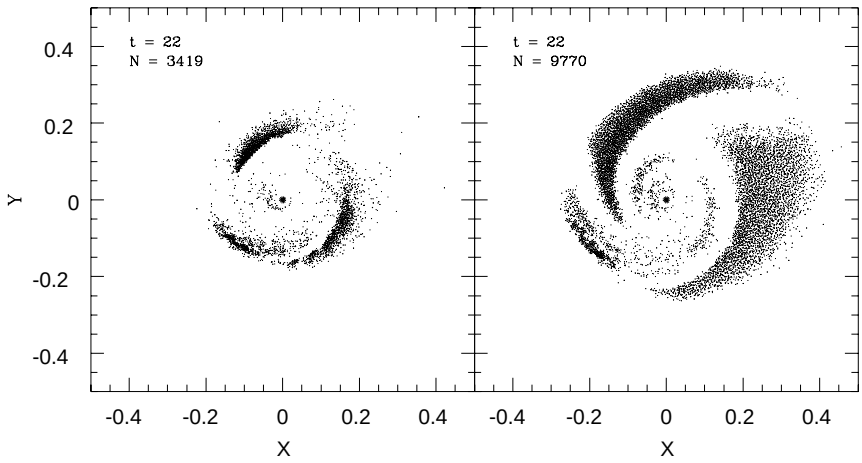

Fig. 2. *XY* plots of the supersonic component in the radial flux of the two accretion disc models. "Inviscid" model is on the left side; the physically viscous one is on the right side. Final time *t* and total particle number *N* are reported.

Lanzafame et al. (2000, 2001) showed that spirals come out in $\gamma = 1.01$ 2D models according to some injection conditions concerning the initial angular momentum and the total energy at the outer boundary at the L1 point. 2D models make the spiral shock development easier because the degradation and smoothing out effects of artificial viscosity are lighter than in 3D models (Monaghan 1985, 1992; Monaghan & Lattanzio 1985). This difficulty has also been admitted by Yukawa et al. (1997) in their 3D SPH simulations where they did not find any spiral as concerns $\gamma = 1.01$ 3D SPH models in sonic or in quasi-sonic injection conditions at L1. Therefore, our previous idea is now confirmed again: high momentum conditions injections – and a highly supersonic injection among these – are quite favourable initial conditions to develop spirals.

4.2. Role of physical viscosity on disc morphology, dynamics and temperature

As is evident from Figs. 1 and 2, the main geometrical effect of physical viscosity is to spread out radially the whole disc on

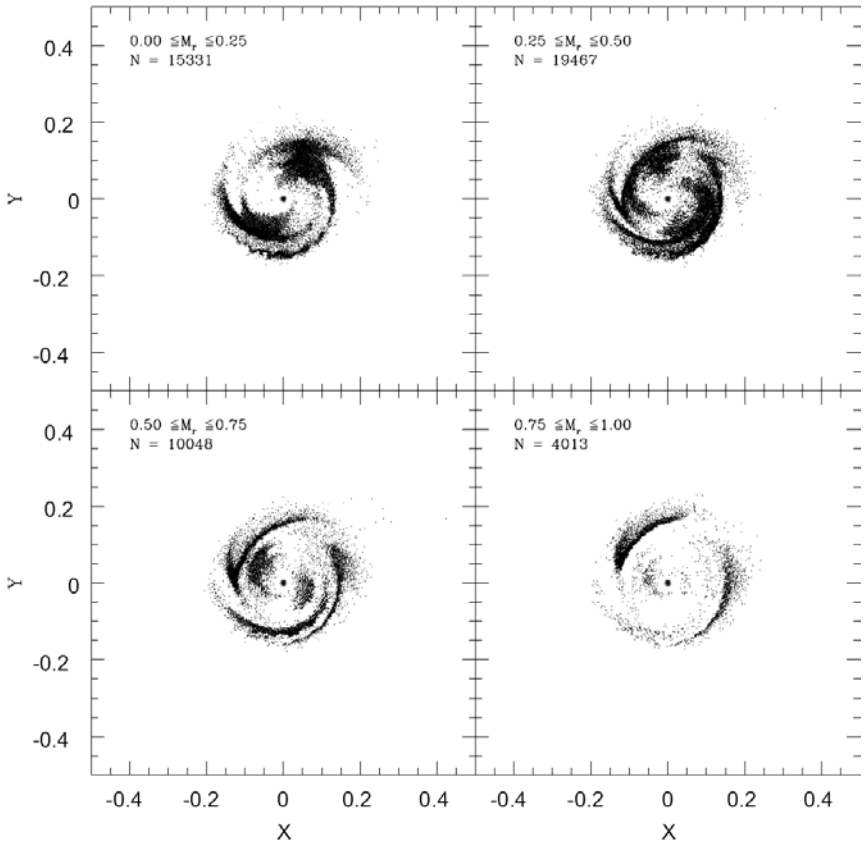

Fig. 3. *XY* plots of the subsonic component only of the "inviscid" SPH accretion disc model. Selections in the radial Mach number M_r have been fulfilled as shown in the four plots. Total particle number N is also reported for each selection.

the *XY* orbital plane. Furthermore, two spirals and spiral shock fronts are also very evident and much more extended from the disc outer edge towards the disc bulk, closer to the primary. A comparison of the radial extension of both disc models is also clear in Fig. 4 where $r_{xy}Z$ plots of the two disc structure models are shown; they are obtained by folding all disc bulk particles onto a plane perpendicular to the orbital plane. The latitudinal angular spread of $\simeq 25^\circ$ of the physically inviscid accretion disc model decreases to $\simeq 15^\circ$ in the case of the physically viscous disc model. Besides the more stretched and slim structure of the physically viscous disc (that is due to the more effective particle radial velocity transport and particle channeling towards the primary), Fig. 4 shows at the same time the supersonic component in the radial flux of both types of discs. The supersonic component confinement at the disc outer edge and onto the two disc surfaces in the physically non-viscous model is, in our opinion, an artificial viscosity effect. Figure 5 completes our analysis as far as discs structure and tangential dynamics are concerned, showing, in logarithmic scales, angular momentum and temperature radial distributions of the two disc models. No clear difference comes out statistically in the tangential dynamics. Both angular momentum radial distributions are very close to that of the standard model $J \propto r^{1/2}$. This can be explained considering that in stationary conditions an accretion disc redistributes angular momentum injected at the outer edge in the disc bulk according to outer edge boundary conditions only, as shown already in Lanzafame et al. (1993) and Belvedere et al. (1993). Physical viscosity plays a role in regions where velocity gradients among particles are meaningful. This means that in an accretion disc, physical viscosity plays a relevant role mainly in the radial transport, while it has scarse influence as far as the tangential dynamics is concerned; of course excluding tangential motions very close to spirals. A strong difference, in spite of the fact that both models treat quasi-isothermal cases ($\gamma = 1.01$), appears when looking at the temperature radial distribution. In fact, the heating effect of the physical viscosity is evident particularly in the disc inner zones. Therefore, the main consequences of both viscous heating and of a more efficient radial particle transport (even along spirals) are the following: disc radial enlargment up to $\simeq$50%, disc thinning as far as their angular spread is concerned, disc heating and, at last, the consequent reduction in disc mass and in disc mean density. Therefore, a relevant result is that hotter particles are much better accreted and channeled onto the primary surface along spirals. This can be also found by looking at Fig. 6 that shows a comparison between the two accretion rates. The conversion factor from particle/time to g s^{-1} is more or less $\simeq \rho_\circ v_\circ (h d_{12})^2$. At $t = 22$ the physically viscous accretion disc model shows an accretion rate close to about twice the value of the physicaly non viscous one. Therefore, as it is evident by counting the total particle numbers, that the "inviscid" accretion disc is nearly twice as massive as the physically viscous one. In our models we did not consider radiative transport, losses and heating. This implies that, taking into

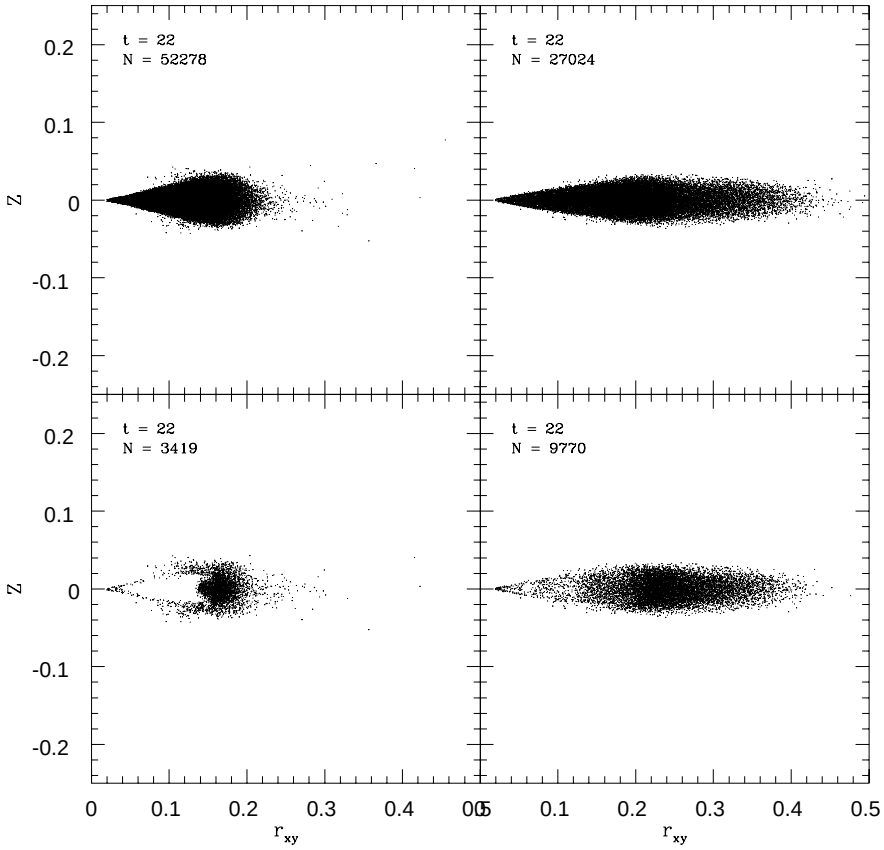

Fig. 4. $r_{xy}Z$ plots of the "inviscid" SPH accretion disc model (left side) and the physically viscous one (right side). $r_{xy}Z$ plots of supersonic component only of the two models are also reported (bottom side). Last time t and total particle number N are reported.

account gas – radiation interaction, radiation coming out from the accretion process, disc radial extension, and disc accretion rates, high viscosity accretion discs should be much bluer and much brighter than non-viscous discs. Obviously, comparing only two models we are not able to write a fine relation describing the connection between the physical viscosity and the mean disc radius. Nevertheless, we can simply conclude, as a linear first approximation, that the mean disc radius $\overline{R}_{\rm d}$ is:

$$\overline{R}_{\rm d} = 0.1\alpha_{\rm ss} + 0.0062q^3 - 0.0227q^2 - 0.0769q + 0.2933 \quad (23)$$

where $q = M_2/M_1$ is the stellar mass ratio between the secondary star and the compact primary star. This relation, in the physically inviscid case ($\alpha_{\rm ss} = 0$), has been written taking into account our previous 2D results (Lanzafame et al. 2000, 2001) as far as the disc mean radius as a function of stellar mass ratio is concerned considering the following four couples of values: ($q = 0.5$, $\overline{R}_{\rm d} \simeq 0.25$), ($q = 1.0$, $\overline{R}_{\rm d} \simeq 0.20$), ($q = 2.5$, $\overline{R}_{\rm d} \simeq 0.15$), ($q = 5.0$, $\overline{R}_{\rm d} \simeq 0.12$). In such papers, each q value is assumed as an initial boundary condition for the four accretion disc models considered, while the corresponding $\overline{R}_{\rm d}$ valuesare evaluated in steady state conditions.

Figure 7 offers a comparison of a normalized hypothetical emission line for both disc models considering three defined orbital phases in the case of optically thin discs. These line profiles are obtained by summing up as many Gaussian line profiles as disc particles. Each Gaussian profile broadening is determined by thermal broadening while each Gaussian shift is determined by the Doppler effect. Tangential motions contribute mainly to Doppler line broadening and to the evident formation of the two reversal peaks. The stronger line asymmetries in the two reversal peaks in the case of physically viscous accretion disc models reflect geometrical asymmetries in disc morphology, whilst the lower line broadening in the same model reflects the reduction of particle density mainly in the inner disc regions. Figure 8, gives a graphical presentation of two disc Doppler tomograms (dDt), one for each model, generated adopting dimensionless velocities. A comparison between our theoretical dDt and some observational dDt, showing spiral structures in cataclysmic variable accretion discs, can be made by looking at Steeghs & Stehle (1999), where nice emission line profiles are also included. The inner edge of an accretion dDt is typically representative of the disc outer edge, whilst the outer edge of an accretion dDt refers to the disc inner edge. This effective analysis offers a good method to discover whether evident spiral structures exist, where they are located and how much they are extended, matching an observational dDt with a Keplerian accretion disc model. Our theoretical dDt allow us to disentangle evident differences in our accretion disc models both in their structure and dynamics and in their geometries. In fact, both outer edge asymmetries of physically viscous accretion disc models and the presence of its two large spirals are clearly distinguishable with respect to the physically non-viscous model.

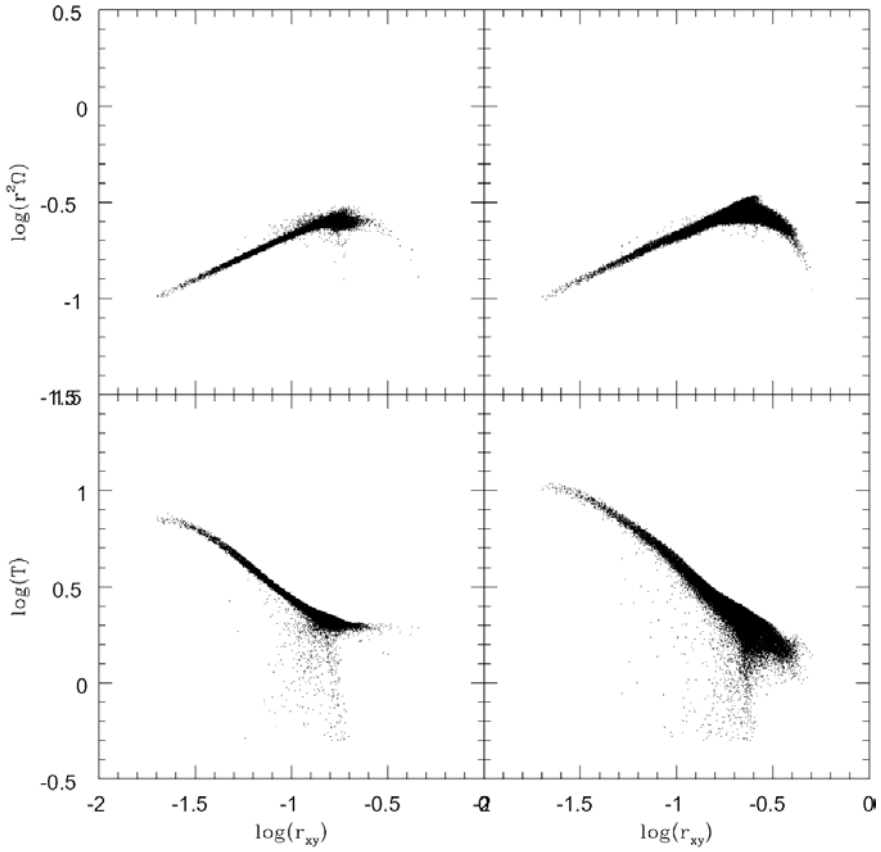

Fig. 5. Angular momentum and temperature radial distributions for both accretion disc models. "Inviscid" model plots are on the left side. Physically viscous model plots are on the right side.

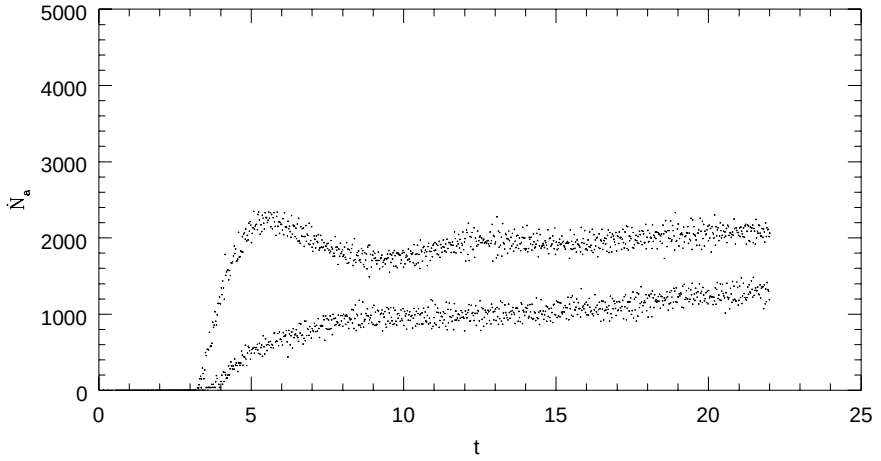

Fig. 6. Accretion rates $\dot{N}_a$ as a function of time t for both accretion disc models. Physically viscous accretion rate is higher than the "inviscid" one.

Our results for the first time confirm that initial angular momentum injection conditions at the disc outer edge are responsible for disc tangential dynamics and for spiral structure and shock front development even in physically viscous discs. These results were not analyzed in Flebbe et al. (1992, 1994), where the authors developed SPH viscous formulations and applied the code to the same numerical tests, showing that the shear component of the stress tensor is proportional to the α_{ss} parameter times the gas pressure, excluding any artificial viscosity contribution. In Bisikalo et al. (2000), adopting an Eulerian finite difference method and various physical viscosities, they found a self consistent solution showing the absence of shock interactions between the stream flowing from L1, the disk body and its outer edge, and the similarity of flow patterns adopting different disc viscosities.

In this paper we confirm that spiral structures and shock fronts are produced in any case adopting different disc viscosities, according to the angular momentum boundary conditions supporting these structures. These results support our previous idea that the main element contributing to spiral and shock

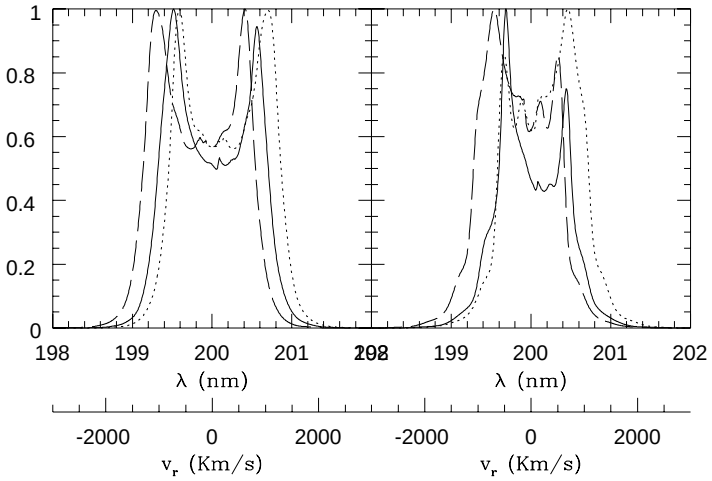

Fig. 7. Hypothetical normalized emission line for both accretion disc models. The "inviscid" model plot is on the left side. Physically viscous model plot is on the right side. Each plot includes three emission profiles according to three orbital phases: superior conjunction – accretion disc in front – solid line; first quadrature – line of sight antiparallel to the *Y* axis – long dashed line; second quadrature – line of sight parallel to the *Y* axis – short dashed line. Radial velocity v_r with respect to the line of sight, as an absolute scale, is also reported.

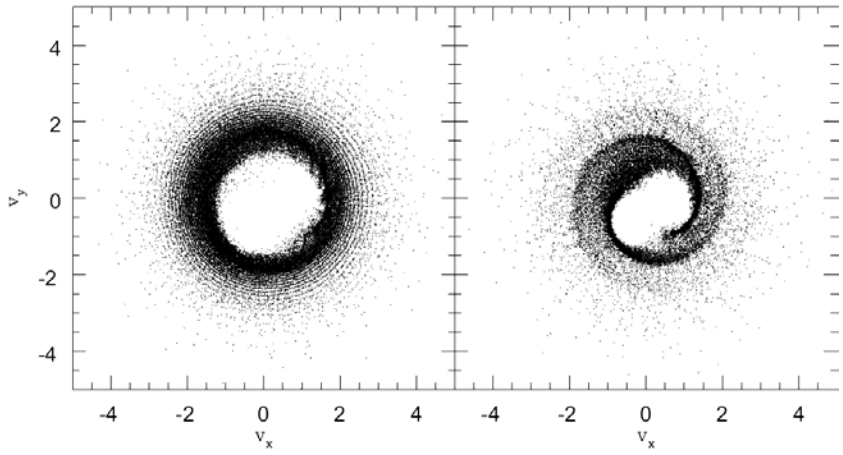

Fig. 8. Accretion disc Doppler tomograms as for the physically non viscous accretion disc model (left) and as for the physically viscous one (right). Dimensionless velocities are adopted.

front development is the starting angular momentum. The inclusion of physical viscosity and, in particular, of a strong physical viscosity, makes the development of a more open spiral pattern easier as a consequence of disc heating, of disc radial expansion into the *XY* orbital plane and of disc thinning. In fact, disc thinning means a better thin disc approximation which, together with disc heating, involves lower supersonic tangential Mach numbers as a function of the radial distance with respect to the physically inviscid disc model. Tangential Mach numbers range from $M_t \simeq 9$ at the inviscid disc outer edge to $M_t \simeq 15$ in the inviscid disc bulk. Instead, they range from $M_t \simeq 8$ at the viscous disc outer edge to $M_t \simeq 11$ in the viscous disc bulk. Therefore, the inclusion of physical viscosity contributes to decrease the radial gradient of M_t. Radial and azimuthal M_t dependence is better plotted in Fig. 9, where as many particles azimuthal distributions of M_t are reported (6) as radial distance selections are shown. Lower supersonic tangential Mach numbers involve more open spiral patterns (Savonije et al. 1994). Finally, tidal effects due to the companion star are certainly much more effective in a larger and more extended accretion disc in the *XY* orbital plane than in a smaller disc. Therefore tidal effects are more effective in a strongly physically viscous accretion disc than in an inviscid one. However, tidal forcing is weakened as M_t increases (Savonije et al. 1994); therefore, large M_t models are less likely to produce spirals.

Another remarkable geometric effect, shown in the *XY* plots of the physically viscous accretion disc model (Figs. 1 and 2), is the stressed *XY* asymmetry in comparison to the physically inviscid disc model. In fact the viscous model enlarges radially and permanently along the positive *X* and along the positive *Y* directions more than along others. Such radial *XY* asymmetry is mainly responsible for one of the two enhanced spiral patterns along the returning particles flow around the primary (which completes a full turn around the primary). We think that strong collisions at the disc outer edge due to the strongly supersonic inflowing stream, combined with disc radial expansion due to the physical turbulent viscosity, better support such asymmetric extension as a consequence of the formation of the spiral pattern directly connected to the injected stream itself. In fact, a large outflowing supersonic particle halo (Fig. 2 – right side)

comes out from the spiral connected to the inflowing stream (between $x \simeq 0.$ and $x \simeq 0.4$) due to the particle collisions between such a spiral with the returning particle flow around the primary. Such a outflowing supersonic halo, supported by disc radial expansion, goes away from the primary towards higher radial distances producing the permanent outer edge distorsion discussed here. Results reported here allow us to conclude that open, wide spirals, as a consequence of viscous radial expansion, are strictly selfconsistently connected to the disc outer edge steady elongation and asymmetry on the opposite side of the impact zone between the disc outer edge itself and the injected stream. On the contrary, tighter spirals should be strictly connected to more symmetric discs.

4.3. Considerations on tidal torques: Their role and limits

Tidal torques in accretion discs of close binaries were originally studied by Papaloizou & Pringle (1977) by using a linear perturbation method for a tidally perturbed flow in the accretion disc by decomposing the tidal perturbation potential into Fourier components. They found that tidal torque is a rapidly increasing function of the radial coordinate r_{XY} in the disc going as r_{XY}^5. Other authors also calculated tidal torques according to different approaches. Zhang & Chen (1992) solved the linear tidal perturbation equation adopting a direct numerical integration method, whilst Ichikawa & Osaki (1994) calculated tidal torques in non-collisional fluid dynamics both according to a linear perturbation method and to a non-linear method based on single periodic particle orbits in the primary Roche lobe, influenced by the binary gravitational potential. All these calculations were performed considering non-collisional fluid dynamics models. In particular, Ichikawa & Osaki (1994) show that tidal effects (i.e. tidal dissipation and tidal torque) are generally small in the accretion disc except beyond or near the "tidal truncation radius", which is given by the largest periodic particle orbit that does not intersect the inner periodic orbit in the disc:

$$\frac{r_{XY}}{d_{12}}|_{\rm t.t.r.} \simeq \left(\frac{2\pi}{c\omega_{\rm orb}} f\right)^5 \qquad (24)$$

where $\omega_{\rm orb}$ is the orbital angular velocity, f is the tidal torque having the dimemsion of $\rm s^{-1}$ and $c\omega_{\rm orb} \approx 0.2 \div 15\ \rm s^{-1}$. This means that the tidal truncation radius generally ranges from $\simeq 0.42 f$ to $\simeq 31.42 f$. According to Paczynsky (1977), to Papaloizou & Pringle (1977) and to Ichikawa & Osaki (1992, 1994), the accretion disc should be tidally truncated very close to the tidal truncation radius in steady state. Once the disc expands radially to the tidal truncation radius, tidal torque should prevent the disc from expanding further. Extra angular momentum transported toward the disc outer edge should be redistributed to the orbital motion of the binary. 2D hydrodynamic simulations of Lin & Pringle (1976), Whitehurst (1989) and Hirose & Osaki (1990) also confirmed this idea. Nothwithstanding this previous idea, Ichikawa & Osaki (1994) themselves admit that: "*full hydrodynamic simulations of accretion disc including the pressure and the viscosity effect are needed for us to understand this phenomenon fully*". In fact, in such 2D simulations, both pressure forces and viscous ones are assumed negligible. Now, in principle, we do not know theoretically a better relation as far as the tidal truncation radius is concerned. It seem that $(r_{XY}/d_{12})_{\rm t.t.r.} \approx 0.30$ at least. As a matter of fact our previos 2D SPH models (Lanzafame et al. 2000, 2001) and the actual 3D physically viscous model seems to confirm such lower limit. This means that if $(r_{XY}/d_{12})_{\rm t.t.r.} \geq 0.30$, spiral patterns and spiral shocks in the radial flow are mainly produced by the initial angular momentum and energy conditions at L1 with a secondary support due to the tidal forces. Moreover, as a second result, $c\omega_{\rm orb} \leq 8$ assuming $f \approx 1$. Instead, if $(r_{XY}/d_{12})_{\rm t.t.r.} \approx 0.20$ at most, tidal truncation effects are not strong enough to prevent the radial disc expansion onto the XY orbital plane as our physically viscous disc model shows.

Recently, an open discussion has come out about the existence or the absence of spiral patterns and possibly of spiral shocks in the radial flux in accretion discs in close binaries. According to some authors, i.e. Bisikalo et al. (1999), Chakrabarty (1992), spiral patterns do not appear if $\gamma > 1.16$ is adopted. Instead, according to some others, such as Matsuda et al. (1990, 1992), Yukawa et al. (1997), Makita et al. (2000), spiral patterns and radial shocks always exist whatever γ is and whatever the initial kinematic conditions are. Recently we wrote some papers (Lanzafame et al. 2000, 2001; Lanzafame & Belvedere 2001; Belvedere & Lanzafame 2002) concluding, via 2D and 3D SPH computer simulations, that initial conditions as far as angular momentum and energy are concerned are crucial in spiral formation. These studies were performed as a consequence of the fact that in some previous papers of ours (Molteni et al. 1991; Lanzafame et al. 1992) we did not obtain spirals both in low compressibility models ($\gamma = 1.1$ and $\gamma = 1.2$) and in high compressibility model ($\gamma = 1.01$), whilst we got spiral patterns, mainly close to the disc outer edge, in Lanzafame & Belvedere (1997, 1998) considering different injection conditions. Of course, in such papers, and also in the present one, we do not hide the difficulty of producing spirals in the disc bulk via SPH because of the smoothing effect of the artificial viscosity, but, if they exist, they should be present at least at the disc outer edge, inside the tidal truncation radius, as we obtained in Lanzafame et al. (2000, 2001) and in the present paper. Yukawa et al. (1997) confirm this difficulty as for $\gamma = 1.01$ 3D SPH simulation at least. Nevertheless, artificial viscosity is necessary in SPH as well as in other Lagrangian methods. It could be reduced, and some authors (Meglicki et al. 1993) worked in such a way performing high compressibility SPH models adopting $\alpha = 10^{-4}$ and $\beta = 0$, but they did not obtain spirals. The next challenge is therefore to build up a SPH code without an explicit artificial viscosity contribution including other fluid dynamic techniques (e.g. Riemann solvers) and adopting a higher spatial resolution, to verify if weak shock fronts develop inside an "inviscid" disc bulk and, secondly, to compare such a disc model with a physically viscous one to understand better the physical viscosity effects. Perhaps this could help us to avoid discussions about the numerical methods adopted. Both in Yukawa et al. (1997) and in Makita et al. (2000), it seems that the inflowing stream is geometrically more similar to the injected particle stream in

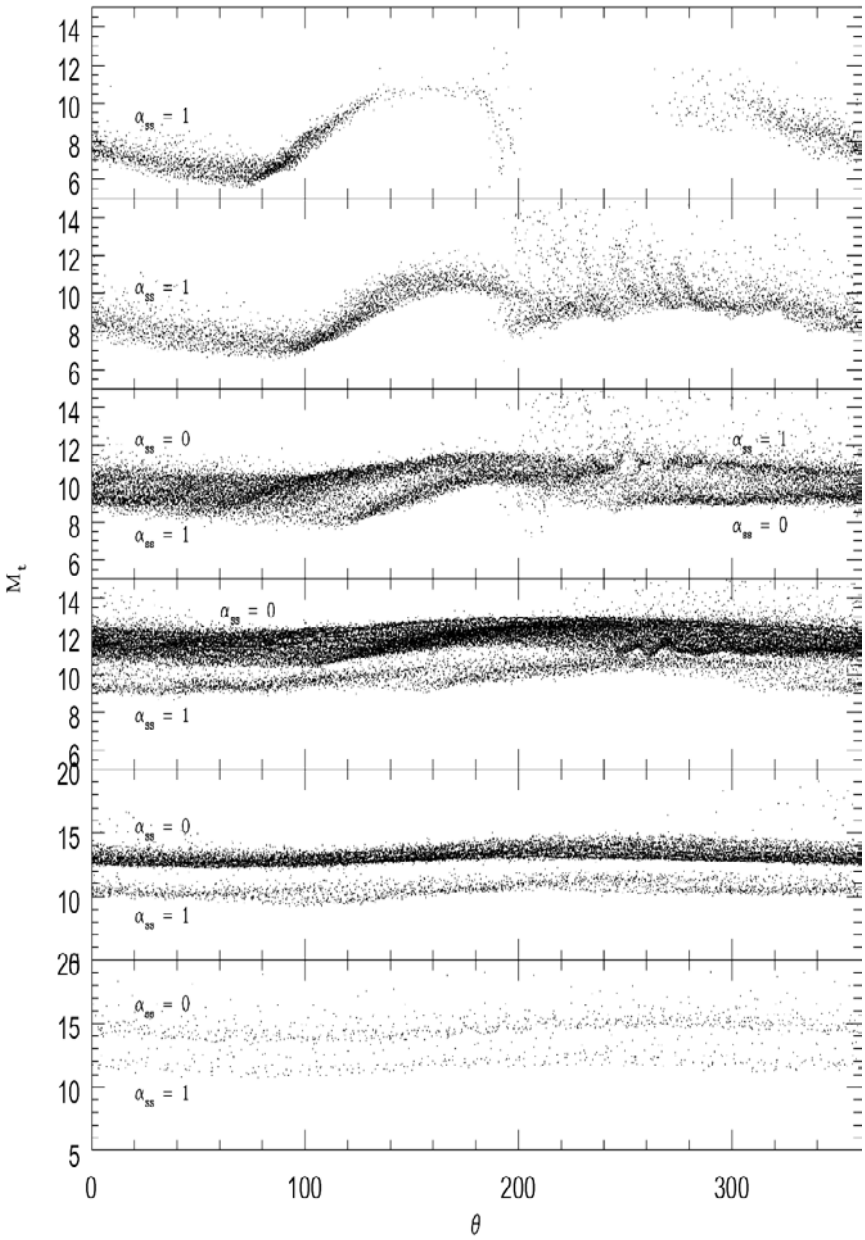

Fig. 9. Azimuthal distribution of tangential Mach number M_t for six radial distance (r) selections. Particles whose $r \leq 0.05$ are reported here in the bottom diagram. Particles whose $0.25 \leq r \leq 0.30$ are here reported in the top diagram. Each shell has $\Delta r = 0.05$ thickness. Both inner radius and outer radius of each shell increase from the bottom to the top. The two α_{ss} values distinguish the two disc models.

Lanzafame & Belvedere (1997, 1998) than to the injected particle stream in Molteni et al. (1991) and in Lanzafame et al. (1992). As a secondary, but minor, consideration in Fig. 1 of Yukawa et al. (1997), it is shown that the SPH filling up rate of the primary Roche lobe is still very high. Therefore, their initial mass transfer conditions seem to be different to those adopted in Molteni et al. (1991) and in Lanzafame et al. (1992). We believe that the problem of revealing spirals is, once more, connected to the initial kinematical, thermodynamical and geometrical mass transfer conditions. Also, it is not a problem of SPH resolution in particular in high compressibility models, as Makita et al. (2000) discuss, because at the disc outer edge (and spirals, if they exist, are resolved there), particle concentration is normally rather low. It is also not a problem concerning the adopted numerical method.

Acknowledgements. We thank Prof. D. Molteni for some helpful suggestions, Prof. G. Bisnovatiy-Kogan and Prof. V. Pirronello for a critical reading of the original version of the paper and for very useful comments that improved the presentation of the paper, Prof. G. Belvedere for helpful financial support in computational resources as well as for interesting comments, and Dr. A. F. Lanza for some helpful discussion about the boundary conditions. Furthermore, in particular we thank the anonymous referee for his/her insight in understanding this paper in its first original version despite the mixed up English and for his/her deep considerations and comments about both the tidal

truncation radius problematics and the disc mean radius dependence on physical viscosity.

References

Belvedere, G., Lanzafame, G., & Molteni, D. 1993, A&A, 280, 525
Belvedere, G., & Lanzafame, G. 2002, PASJ, 54, 781
Bisikalo, D. V., Boyarchuk, A. A., Kuznetzov, O. A., et al. 1998a, Astron. Rep., 42, 33
Bisikalo, D. V., Boyarchuk, A. A., Chechetkin, V. M., Kuznetzov, O. A., & Molteni, D. 1998b, MNRAS, 300, 39
Bisikalo, D. V., Boyarchuk, A. A., Chechetkin, V. M., Kutznetsov, O. A., & Molteni, D. 1999, Astron. Rep., 43, 797
Bisikalo, D. V., Boyarchuk, A. A., Kutznetsov, O. A., & Chechetkin, V. M. 2000, Astron. Rep., 44, 26
Blondin, J. M. 2000, New Astron., 5, 53
Boris, J. P., & Book, D. L. 1973, J. Comput. Phys., 12, 1198
Chakrabarty, S. K. 1992, MNRAS, 259, 410
Drimmel, R. 1993, MNRAS, 282, 982
Flebbe, O., Münzel, H., Riffert, H., & Herold, H. 1992, Mem. Soc. Astr. It, 65, 1049
Flebbe, O., Münzel, H., Herold, H., Riffert, H., & Ruder, H. 1994, ApJ, 431, 754
Hirose, M., & Osaki, Y. 1990, PASJ, 42, 135
Ichikawa, S., & Osaki, Y. 1992, PASJ, 44, 15
Ichikawa, S., & Osaki, Y. 1994, PASJ, 46, 621
Kaisig, M. 1989, A&A, 280, 525
Landau, L. D., & Lifshitz, E. M. 1959, Course of Theoretical Phisics, vol. VI: Fluid Mechanics (Pergamon Press)
Lanzafame, G., Belvedere, G., & Molteni, D. 1992, MNRAS, 258, 152
Lanzafame, G., Belvedere, G., & Molteni, D. 1993, MNRAS, 263, 839
Lanzafame, G., & Belvedere, G. 1997, MNRAS, 284, 957
Lanzafame, G., & Belvedere, G. 1998, MNRAS, 295, 618
Lanzafame, G., Maravigna, F., & Belvedere, G. 2000, PASJ, 52, 515
Lanzafame, G., Maravigna, F., & Belvedere, G. 2001, PASJ, 53, 139
Lanzafame, G., & Belvedere, G. 2001, JKAS, 34, S313
Lattanzio, J. C., Monaghan, J. J., Pongracic, H., & Schwarz, M. P. 1986, SIAM J. Sci. Stat. Comput., 7, 591
Lin, D. L. C., & Pringle, J. E. 1976, in Structure and Evolution of Close Binary Systems, ed. P. Eggleton, S. Mitton, & J. Whelan (Dordrecht: D. Reidel Publishing Company), IAU Symp., 73, 237
Makita, M., Miyawaki, K., & Matsuda, T. 2000, MNRAS, 316, 906
Matsuda, T., Sekino, N., Shima, E., Sawada, K., & Spruit, H. 1990, A&A, 235, 211
Matsuda, T., Ishii, T., Sekino, N., et al. 1992, MNRAS, 255, 183
Molteni, D., Belvedere, G., & Lanzafame, G. 1991, MNRAS, 249, 748
Meglicki, Z., Wickramasinghe, D., & Bicknell, G. V. 1993, MNRAS, 264, 691
Monaghan, J. J. 1985, Comp. Phys. Rept., 3, 71
Monaghan, J. J. 1992, ARA&A, 30, 543
Monaghan, J. J., & Lattanzio, J. C. 1985, A&A, 149, 135
Murray, J. R. 1996, MNRAS, 279, 402
Paczynsky, B. 1977, ApJ, 216, 822
Papaloizou, J. C. B., & Pringle, J. E. 1977, MNRAS, 181, 441
Savonije, G. J., Papaloizou, J. C. B., & Lin, D. N. C. 1994, MNRAS, 268, 13
Sawada, K., Matsuda, T., Inoue, M., & Hachisu, I. 1987, MNRAS, 224, 307
Sawada, K., & Matsuda, T. 1992, MNRAS, 255, 17
Shakura, N. I. 1972, Astron. Zh., 49, 921 (English tr.: 1973, Sov. Astron., 16, 756)
Shakura, N. I., & Sunyaev, R. A. 1973, A&A, 24, 337
Spruit, H. C., Matsuda, T., Inoue, M., & Sawada, K. 1987, MNRAS, 229, 517
Steeghs, D., & Stehle, R. 1999, MNRAS, 307, 99
Truss, M. R., Murray, J. R., Wynn, G. A., & Edgar, R. G. 2000, MNRAS, 319, 467
Truss, M. R., Murray, J. R., & Wynn, G. A. 2001, MNRAS, 324, L1
Whitehurst, R. 1989, in Theory of Accretion Discs, ed. F. Meyer, W. J. Duschl, J. Frank, & E. Meyer-Hofmeister (Dordrecht: Kluwer Academic Publishers), 213
Yukawa, H., Boffin, H. M. J., Matsuda, T., & Inoue, M. 1997, MNRAS, 292, 321
Zhang, Z. Y., & Chen, J. S. 1992, A&A, 261, 493